Rev. Roum. Sci. Techn.– Électrotechn. et Énerg.
Vol. **71**, *2*, pp. 323–328, Bucarest, 2026

RECREATION OF THE INDEX METACARPAL BONE USING 3D PRINTING FROM RADIOLOGICAL

SUNDARAM RAMKUMAR[1], MUTHUSAMY RAJEEV KUMAR[2]

Keywords: Fracture; X-ray; Index metacarpal bone; Regeneration; 2D Image; 3D Printing; Calcium hydroxyapatite.

Accidents often cause fractures, and since bone regeneration is difficult, the loss can be replaced with artificial bones. The article aims to replace the original bone model using radiographic-based replacement techniques. The radiographic image (2D) of that particular fractured bone is converted into the 3D structure. Since radiographic images are 2D, they are converted into 3D using image processing techniques. The process involved replacing the new bone structure by converting a 2D X-ray image into a 3D model using MATLAB and CATIA. In this process, the following image processing techniques are used: grayscale conversion and K-Means clustering-based Segmentation. Finally, the CATIA software is used to obtain the required 3D image of the metacarpal bone to be replaced. Finally, using a 3D printer, the metacarpal bone 3D structure was created from calcium hydroxyapatite, measuring 56.33 mm in length.

1. INTRODUCTION

In the last two centuries, technology has attempted to compete with nature, but nature proves its royalty then and there in the world. This research article is one such experiment aimed at competing with nature. Generally, babies have a bone count of 300+, and over time, the skeletal structure fuses, reaching a count of 206 bones between the ages of 18 and 25 years [12]. The soft tissues in the human body that support the skeletal system and bones are a combination of dense connective tissues and hard tissues that form the bone structure. Bone tissue is a special type of tissue due to its cellular organization and the composition of various minerals. These reasons make the bone a rigid organ in the human body. The bones of toddlers are less rigid, so they have a high elasticity, leading to a lower fracture rate [13]. Rigidity and age are inversely related, so the fracture rate can be high in adults and older people.

A bone fracture is not a disorder, and it is a discontinuity in the bone structure, such as a mild or linear crack [16], a break, or complete breakage or partial breakage, and sometimes the bone may be broken into bits and pieces. An unbearable stress force or impact acts on a particular bone, which may lead to a fracture. The stress factor varies among different types of bones, such as sesamoid, flat, irregular, short, and long bones. Usually, long bones fracture because they are weight-bearing and are located throughout the body, such as the legs, arms, and shoulders [25].

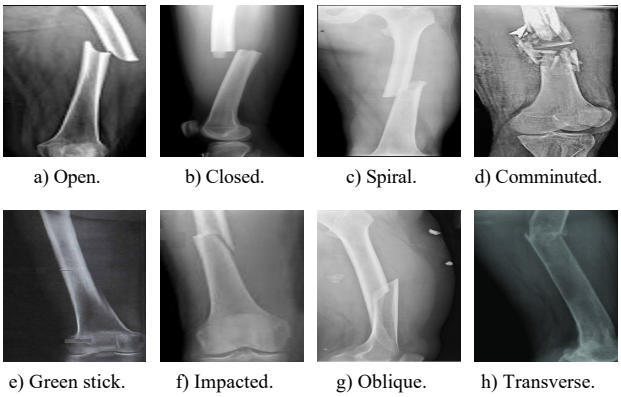

a) Open. b) Closed. c) Spiral. d) Comminuted.

e) Green stick. f) Impacted. g) Oblique. h) Transverse.

Fig. 1 – Possible ways of bone fracture.

Reasons for the fractures are impact due to a fall (Stress), an accident creates a high force in the bones, and pathological or disorder conditions such as osteoporosis, osteopenia, bone cancer, osteogenesis imperfecta, and a lot more. Fracture also refers to small and tiny cracks in bone structure, and the crack or breakage in the bone can happen to any of the bones in the skeletal system. Bone fractures can occur in two ways: the first way through accident, and the second way because of a lack of bone minerals. The fracture can occur in 8 different ways, and it is classified according to the degree of bone breakage and its angle. Closed, open, comminuted, spiral, oblique, green stick, impacted, and transverse are the possible ways a bone gets fractured, as shown in Fig. 1. Some of the fractures are mid and effortlessly curable, such as closed, spiral, oblique, green-stick, and impacted [16]. Medical professionals might recommend using an X-ray [8] imaging method to determine the fracture's impact. An MRI or CT scan may be necessary in a few complex cases to determine the fracture's impact [1]. (Immobilization). The fractures may be treated with procedures such as stem cell therapy, ultrasound therapy, and bone grafting. The bone graft is a great technique that replaces the original bone with artificial bone. An article presents an artificial bone creation process. This article focuses on manipulating the missing bone area from a fracture and constructing a 3D model of a broken bone from a 2D medical image [24].

2. LITERATURE SURVEY

Sunanda et al (2019) suggested a method in machine learning for converting 2D to 3D that is independent of the experiment setup. Singh (2007) suggested a method with CT scan, and it delivers 3D information of the internal organs, but this method is not chosen mostly because of high radiation. Phan (2011), femoral fractures due to high force is act on the bone, hence the bone experiences breakage. Radiographic imaging was performed with the help of X-rays to observe the structure of the internal bone matrix, and based on the radiographic images, transplantation can be provided to the subject. Konrad (2012) proposed a conversion method for 2D imaging to a 3D image with the help of a computer algorithm, and the 3D image was not trained because the validation was restricted to a database of indoor scenes, and the images were not completely void of distortions. Uros Mitrovic (2013) suggested 3D to 2D rigid regeneration with the help of a cerebral angiograms algorithm, and this algorithm is to find the orientations with

[1] Department of ECE, Sri Eshwar College of Engineering, Coimbatore, India-641202.
[2] Department of CSE, Vel Tech Rangarajan Dr. Sagunthala R&D Institute of Science and Technology, Chennai, India- 600062.
Emails: ramkumar.s@sece.ac.in, drmrajeevkumar@veltech.edu.in

DOI: 10.59277/RRST-EE.2026.2.26

intensity-matched gradient similarity. Chenxi Zhang (2014) proposed an automatic method for automatically detecting different types of movements in the bone. Divya and Sneha Arun (2014) proposed a method for converting a 2D image to a 3D image with the help of a video conversion technique, and it is one of the ways of using depth maps-based rendering. Huang (2015) suggested a naturalistic method for 2D image -3D image, and this was performed by NSSs (Natural scene statistics). The following details were deliberated: compensation processes, depth information, and depth initialization. Jyoti Yadav (2013) proposed a method to apply the K-Means Clustering algorithm. Jiajun Wu (2018) proposed a model that reconstructs a 3D image from a single RGB image and represents a single view of 3D. Indu Yekkala (2018) proposed extracting patterns and associations from this large volume of data to perform tasks more quickly and effectively [15].

3. MATERIALS AND METHODS

3.1 NEED FOR ARTIFICIAL BONE

Artificial bone is like an original bone, but it is tailor-made in a laboratory that can be used as a replacement for congenital deformities, bone tumors, bone fractures, or as part of joint replacement surgeries [16]. Bones that are weak or shattered can be stabilized and supported with artificial bones. They can be used to keep broken bones together as they heal, enabling the body's own processes for bone re-growth to occur. Artificial bones are employed in clinical trials, as well as to evaluate the efficacy and safety of different medical equipment and surgical techniques. These models can help advance surgical methods and medical equipment by mimicking the behavior of actual bones. Artificial bones can act as scaffolds to support the development of new bone tissue. These structures are used by researchers to build biocompatible frameworks for bone regeneration in individuals with severe bone deformities. Generally, bone has a self-repair system that is referred to as the resorption process. There are two important cells that help to etch the old bone cells (osteoclasts) and new bone cells that are grown in the same location (osteoblasts). In the case of server damage, the bone resorption process may not help the bone restore its original structure and shape. The skeletal system is unable to regenerate the bone losses, so orthopedic surgeons may conclude to replace the damaged bone with an artificial bone with the help of allografts, autografts, and synthetic grafts. The tools and techniques for identifying finger vein patterns are discussed in this article (Table 1).

Table 1

Comparison of different artificial bone techniques.

Categories	Allografts	Auto-Grafts	Synthetic Grafts
Biocompatible	Moderate	Moderate	High
Invasive	Less	Less	High
Osteoconductivity	High	Less	High
High porosity	Less	High	Less
Biomechanics	Less	Less	Less

In the proposed system, the vein pattern images were used because of their easy and simple algorithmic structures. The vein pattern: 50 samples were collected from the database and processed using MATLAB software. Since images are in (2D) two dimensions, they are processed in the multidimensional systems for conversions [14,17]. Digital image processing helps for many applications in terms of projections, feature extractions, pattern recognition, multi-scale signal analysis, classification, and a lot [9].

3.2 DIAGNOSTICS PROCESS

Step 1: Image acquisition (a sensor or camera takes the picture) and digitization (an analog-to-digital converter turns the image into a digital format). Step 2: Image Enhancement, manipulating the image in terms of pixels or colors so that information extraction is easier than in the original image, and highlighting features in the image. Step 3: Image restoration is the process of enhancing an image's look using mathematical or probabilistic models (Fig. 2). Step 4: Color Image Processing –extraction of the features from an image based on the RGB ratio. Step 5: Wavelets: utilized for image data compression, they degrade images in different degrees of resolution. Step 6: Compression Techniques- Used for reducing the disk storage of the image, making it comfortable for transmitting and receiving the image. Step 7: Morphological Processing is useful in the description and representation of shape. Step 8: Image Segmentation, partitioning of the image into bins or windows. Step 9: Description – Representation: Representation of the image as a complete region or as a boundary. Boundary Representation can be focused on exterior shape properties of the image, like inflections and corners. Region Representation can be focused on exterior shape properties of the image, like texture or pattern.

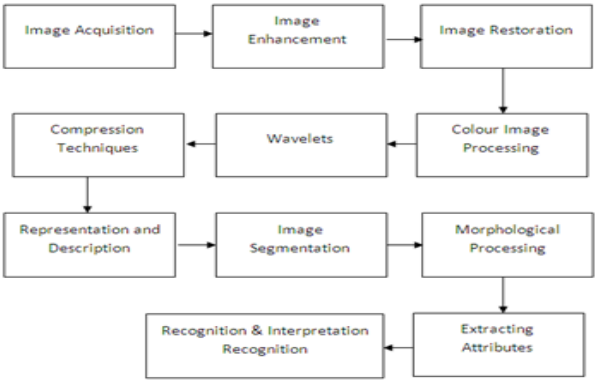

Fig. 2 – Flowchart of the digital image processing.

Step 10: Representation and Description: Selecting a representation is only one stage in transforming unprocessed data into a format that computers can further process. Step 11: Recognition and Interpretation. Recognition: assigning a label to the object based on the description.

3.3 RECONSTRUCTIONS OF BONES

The heated reservoirs provide the raw materials for printing, and the fused deposition modeling (FDM) printer heads begin releasing them for 3D printing [7]. 3D FDM printing was used to build the artificial bone, and this was achieved by reconstructing an X-ray image obtained from the subject [1]. The artificial bone was not created with a 3D bio printer, but the aim is to develop a 3D structure of the metacarpal bone with a 2D image. Based on the resolution, the 3D bone model can be divided into different layers. The printer starts to build layer by layer to achieve the outcome of the artificial bone model [6,18]. As per the literature survey, calcium hydroxyapatite (HA) nanocrystals are the ultimate raw material for the FDM printer to build artificial bones. Applications for artificial bones derived from calcium hydroxyapatite include spinal fusion, bone grafting, and

orthopedic implants.

A few of calcium hydroxyapatite's characteristics, including osteoconductivity, biocompatibility, mechanical properties, biological similarity, and slow biodegradation, make it easier to use in the fabrication of artificial bones (Fig. 4). This calcium hydroxyapatite is suitable for all ages and both male and female genders. DICOM data was not used in this article for validation. When using calcium hydroxyapatite as a material to create artificial bone in medical procedures, there are several potential side effects and complications to be aware of. These include the possibility of infection, though this risk can be minimized by using proper sterile techniques during implantation; localized inflammation or swelling at the implant site; prior to the procedure, subjects should be screened for allergies or sensitivities to calcium hydroxyapatite; and mild to moderate pain or discomfort at the implant site. The volume of calcium hydroxyapatite may decrease over time due to gradual resorption or degradation [26].

Table 2

Comparison between calcium hydroxyapatite material and different types of bones.

Mechanical Properties	Calcium Hydroxyapatite Material	Short Bone	Long Bone
Tensile Strength,	38.0 - 48.0 MPa	5 to 20 MPa	130 to 180 MPa
Shear Modulus	2.76 - 5.12 GPa	3 to 6 GPa	4 to 12 GPa
Flexural Strength	100 - 120 MPa	50 to 150 MPa	120 to 180 MPa
Compressive Strength	350 - 450 MPa	10 to 30 MPa	100 to 200 MPa
Poisson Ratio	0.27	0.25 to 0.35	0.25 to 0.35
Modulus of Elasticity	7.00 - 13.0 GPa	10 to 30 GPa	14 to 20 GPa

In contrast to the long bone type, the calcium hydroxyapatite material is considerably more appropriate for the short bone type, according to Table 2 values. Although calcium hydroxyapatite's flexural strength value does not fulfill the requirements of long bone types, it is ideal for short bone types. Since the metacarpal bone is a short bone type, reconstructed metacarpal bones are made of calcium hydroxyapatite [28]. The precise application, the patient's overall health, and the body's reaction to the material can all affect how long calcium hydroxyapatite implants or grafts last. Some patients may not have any problems with these implants for the rest of their lives, but over time, others may need replacement or additional care. Patients should monitor and manage the longevity and function of calcium hydroxyapatite implants or grafts by following their dentists' and healthcare experts' advice. Depending on the type of medical or dental surgery and the patient's particular circumstances, different follow-up and care recommendations may be made [26,27].

4. RESULT AND DISCUSSION

The raw material must be pre-processed before the printing with HA nanocrystals, and it should be synthesized by the wet synthesis method along with calcium precursors, calcium chloride, phosphorus, and diammonium phosphate. As an alternative to patching broken bones, 3D printing technology could create implants tailored to specific repair requirements [2]. Implants created using 3D printing techniques have adverse effects on subjects due to variation in host cells' lymphocytes. This demerit can be overcome using polycaprolactone (PCL), which can serve as a replacement for HA nanocrystals in FDM printers. The 3D model of the bone is provided to the 3D printer in the (.STL) format (Fig. 3). The printer then prints the 3D model of the bone, with the material inserted [3,4]. First, the input image is processed in MATLAB (MATLAB R2021b), and then in CATIA for the 3D bone model [30]. Finally, the processed 3D model image is then used to print the 3D model bone using a 3D printer (Fig. 4).

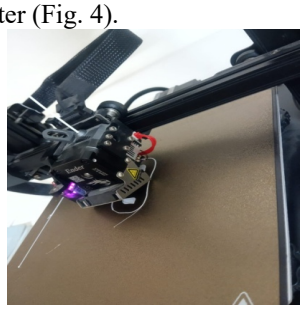

Fig. 3 – FDM printing machine.

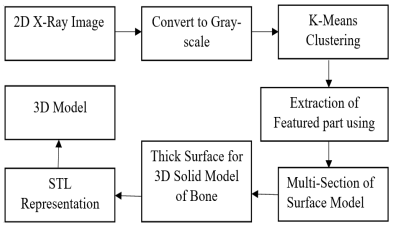

Fig. 4 – Stages of conversional 3D bone modeling.

Fig. 5 – Raw bone image considered as input image.

The raw 2D X-Ray input image (Fig.5) is converted into a grayscale image, and all X-ray images are grayscale images, but once it has been converted into a grayscale image, the pixel values can be uniformly distributed, hence the noise ratio can be reduced, and further, the grayscale noises were removed [11]. The K-Means clustering algorithm groups pixels that are similar to each other. Re-estimating the clusters means, the same procedure is repeated over and over to attain the stable cluster and working procedure of the k-means algorithm as follows: This algorithm randomly selects a point "k" as the primary cluster centroids; The closeness will be verified from the "k" point of the input dataset based on the Euclidean distance [10]; Each cluster centroid distance is estimated once again as the average of the points. Codes for cluster formation as foreground and background, hence, bone regions from the processed image can be clustered.

```
# defining the k-means function with initialization as k-means++
"kmeans = KMeans (n_clusters=2, init='k-means++')
```

void
fitting the k means algorithm on scaled
data kmeans.fit (data_scaled)"

The first two steps were repeated until the clusters diverged, and finally, if there were no changes observed between the clusters, then the cluster group could be defined. The fractured bone was separated with the help of CATIA software. The surface model of the bone was extracted, and multi-sectioning of the surface model was obtained. The surface model is in .jpeg format, which was converted to. STL format, which converts low-dimensional data into higher dimensions using an STL viewer. This software was used to view the data in 3D (3 Dimensions). As an input, we have taken an X-ray image of a fractured index metacarpal bone as a whole finger bone X-Ray. The input image is uploaded to MATLAB. The image processing techniques that are used in MATLAB are Gray-scale imaging and K-means clustering-based segmentation. The results of the K-Means clustering approach are shown in Fig. 6, where pixels with similar intensities are clustered to extract the bone region and eliminate undesirable regions from the input image, such as muscles, nerves, and voids, to obtain feature or depth information [10]. The processed images are classified into two parts: foreground (bone region) and background image, one as bone and the other as background, shown in Fig. 6 [5].

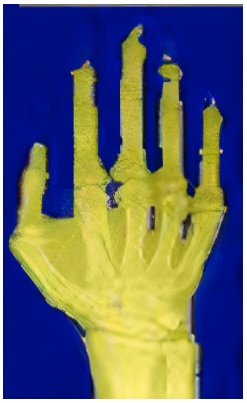

Fig. 6 – Similar intensities are clustered together to extract the bone.

4.1 3D PRINTING OF THE ARTIFICIAL BONE

CATIA v5 was developed by Dassault Systèmes, which is used for computer-aided engineering applications and makes it appropriate for intricate and sophisticated product design. To produce complex and accurate designs, it enables surface, solid, and parametric modeling. CATIA v5 can produce two variants, such as parametric and non-parametric 3D models, as shown in Fig. 7.

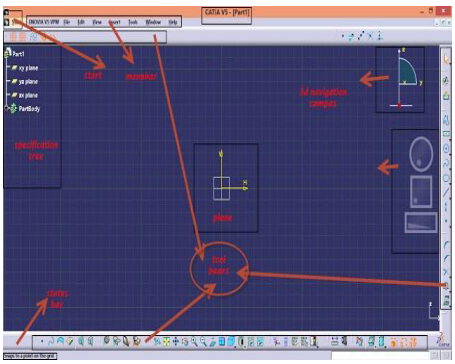

Fig.7 – Surfaces can be modeled through CATIA.

Sketching and Tracing of the imported image can be done using this tool. In this step, the fractured bone can be identified, and preliminary coordinates (Fig. 8a) were created and then traced for the generation of wireframes (Fig. 8b) for the 3D model, and the index metacarpal fractured bone was created as shown in Fig. 8c.

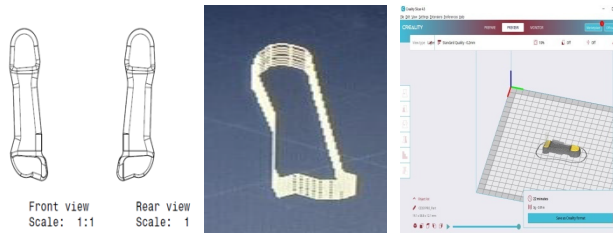

a. Preliminary coordinates. b. Wireframes. c. Pre-final version.

Fig.8 Index metacarpal fractured bone CATIA model

Operation Toolbar: once a profile for the recreation of fractured bone was generated, and the recreation was customized to reach 100 % similarity to the original bone with the help of a couple of commands, such as mirror, trim, chamfer, and a lot more.

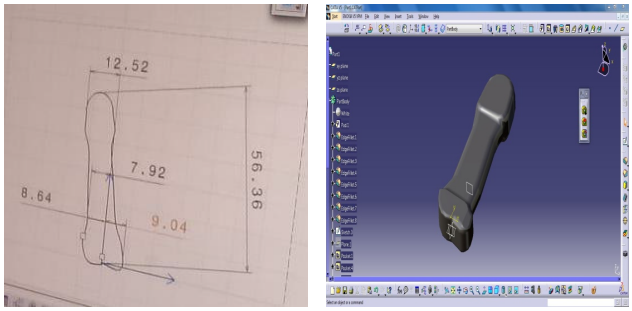

a. Dimensions of metacarpal bone. b. Final version of metacarpal bone.

Fig. 9 – geometrical and dimensional constraint of index metacarpal fractured bone- height 56.36 mm, 7.92 middle width, 12.52 top width and bottom width is 8.64 respectively

Using the constraint toolbar, the profiles were controlled similarly to the original bone structure, such as tangent, parallel, and many others (geometrical constraints), or distances, angles, and many others (dimensional constraints). Following verification of the bone's dimensions and drafting, a 2D machine drawing is produced for the 3D part models. Sweeping two or more section curves along an automatically calculated or user-defined spine can produce a multi-section surface that respects one or more guide curves. The artificial bone geo-dimension was derived as a height of 56.36 mm, a middle width of 7.92 mm, a top width of 12.52 mm, and a bottom width of 8.64 mm, respectively (Fig. 9). The printed metacarpal bone lacks anatomical accuracy due to the thickness expansion during basic 2D segmentation, which causes loss of key morphological details. Henceforth, the model is suitable for numerical analyses such as FEM-based structural studies rather than for direct bone replacement applications.

4.2 THICK SURFACE FOR SOLID CONVERSION

The conversion of the surface of the bone model to the 3D solid model can be done using this tool, which can create the 3D output of the bone that can be exported in an STL file for

the 3D printing of the particular bone, which is known as an artificial bone, as shown in Fig. 10.

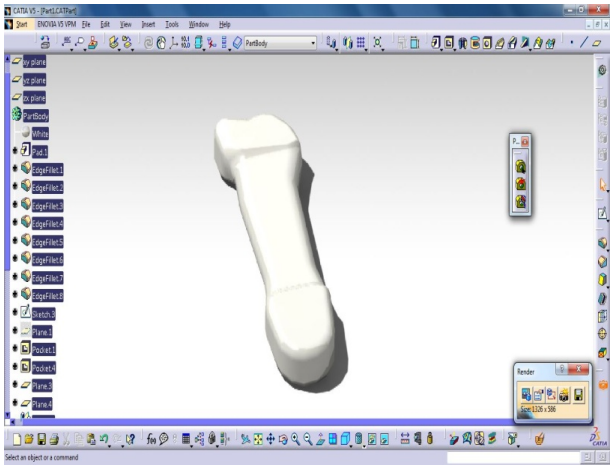

Fig. 10 – 3D output of the index metacarpal bone image extracted from the CATIA software as a screenshot.

The original image from the database is enhanced by increasing the brightness and other properties of the image. Extraction of required data for recreation of bone using an FDM 3D printer and validation was done with the NICE (National Institute for Health and Care Excellence that publishes a range of studies, guidelines, and suggestions on clinical therapies, medical technologies, and healthcare-related subjects) report, as per the standard National Library of Medicine (US-2020) as shown in Fig. 13.

This research produces accuracy with less processing time and cheap availability as compared to existing methods and an easy and cost-effective approach for converting a 2D X-ray image into 3D models, which can be printed by using FDM 3D printers, as shown in Fig. 11. One essential feature of calcium hydroxyapatite and other biomaterials used in bone implantation and regeneration is osteoconduction [24].

The capacity of calcium hydroxyapatite to act as a scaffold for the development of blood vessel ingrowth and attachment, as well as osteoblast cell growth, which results in the creation of new bone tissue [23,29].

Fig. 11 – Recreated artificial index, metacarpal bone model.

4.3 TIME CALCULATION FOR 3D PRINTING

To estimate how long a 3D printing job will take to complete, the 3D printing time must be calculated. The complexity of the design, layer height, print speed, and kind of 3D printer being used are some of the variables that affect how long 3D printing takes. The epiphysis part of the bone takes more time to print, whereas the diaphysis part takes comparably less time for printing, as shown in Fig. 12.

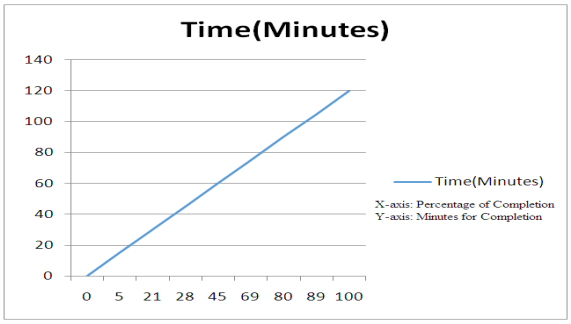

Fig. 12 – Comparison between time and completion status.

4.4 ACCURACY AND VALIDATION ASSESSMENT

Table 3 shows the different parameters of the recreated artificial index metacarpal bone. The artificial bone, as shown in Fig. 11, is recreated using calcium phosphate because it possesses good osteoconductive properties.

Table 3

Dimensions of the recreated artificial bone.

S. No.	Parameters of the index metacarpal bone	Dimensions of the index metacarpal bone [mm]
1	Total Length	56.36
2	Head of the bone	12.52
3	Body of the bone	7.92
4	Base of the bone	8.64

The ability of bone to flex under pressure or stress and then revert to its original shape after the weight or stress is removed is known as its elasticity [20,21]. The elastic modulus of the reconstructed bone is comparable to that of the original bone [19,22].

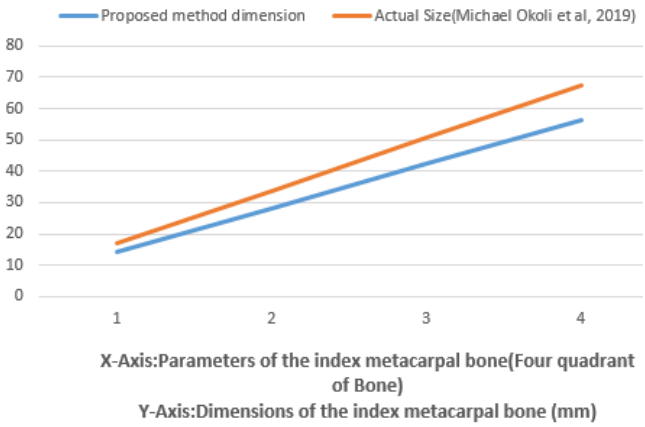

Fig. 13 – Comparisons between artificial printed bone and actual bone (Michael Okoli et al, 2019).

Figure 13 shows the validation comparison between artificial printed bone and actual bone in a graphical mode (Michael Okoli et al, 2019). According to Michael Okoli et al (2019, they analyzed almost 57 subjects and 223 metacarpal bones and produced matrices on the dimensions of the metacarpal bones [13]. They found that the index metacarpal bone is the longest, and the average length is 67.6 mm. They haven't printed a 3D model, but they suggested the dimensions of the metacarpal bone. From their measurements and findings, the proposed 3D artificial bone dimensions were compared. This proposed methodology recreated the index metacarpal bone with a length of 56.36 mm, which is much closer to the length of 67.6 mm. The

difference between the recreated artificial bones is about 11.24 mm. The X-ray image that was used as an input image or source image was taken from an Indian-origin male subject. The bone growth may vary between different nationalities. The average length of the index metacarpal bone is 67.6 mm, which was recorded from Swedish origin, and the average height of males and females is about 179.73 and 165.6 cm, respectively; however, the average height of males and females in India is about 177 and 162 cm, respectively. Thereby, the difference of 11.24 mm in the length of the index metacarpal bone can be considered.

5. **CONCLUSION**

The article focused on recreating a fractured human bone into a more developed 3D model as an artificial bone using a biocompatible material. With this artificial bone, patients were able to live normal lives. The bone obtained by this method will be in accurate dimensions to the original bone. The index metacarpal bone was recreated. The index metacarpal bone recreated with the total length of 56.36 mm; the head of the bone width is 12.52 mm, the body of the bone width is 7.92 mm, and the base of the bone width is 8.64 mm. The achieved outcomes show that the 3D conversion was performed with high accuracy and validated by the NICE report. This article has attempted to reconstruct the fractured bone using a 3D model to replace the fractured portion. Further, this method can help create models of other body parts, such as the ribcage, skull, and more, which can be used to analyze and reconstruct 3D models for better understanding and replacements. This article can also be useful for designing rigid artificial organs, such as teeth and nails, which can be used for replacement, and physicians will be able to make an accurate decision about the replacement of fractured bones.

CREDIT AUTHORSHIP CONTRIBUTION STATEMENT

SUNDARAM RAMKUMAR: methodology, software, original draft preparation, investigation & data curation

MUTHUSAMY RAJEEV KUMAR: conceptualization, visualization & writing- reviewing and editing

Received on 5 April 2025

REFERENCES

1. A. Mehranian, M. Reza, A. Rahmim, H. Zaidi, *3D prior image constrained projection completion for X-ray CT metal artifact reduction*, IEEE Transactions on Nuclear Science, **60**, *5*, pp. 3318–3332 (2013).
2. G.C. Anzalone, C. Zhang, B. Wijnen, P.G. Sanders, J.M. Pearce, *A low-cost open-source metal 3-D printer*, IEEE Access, **1**, pp. 1–10 (2013).
3. C. Zhang, *Inhibition of furin by bone targeting super paramagnetic iron oxide nanoparticles alleviated breast cancer bone metastasis*, **6**, *3*, pp. 712–720 (2020).
4. K.P. Divya, S. Arun, *A survey on 2D to 3D image and video conversion techniques*, International Journal of Research in Advent Technology, **2**, pp. 99–102 (2014).
5. S. Dixit, V.G. Pai, K. Agnani, V.S.R. Priyan, V.C. Radrigues, *3D reconstruction of 2D X-ray images*, pp. 1–5 (2019).
6. H.S.M. Haugen, *Discover the body 3D printing and teaching materials for blind and visually impaired children*, Future Reflections, pp. 1–10 (2013).
7. J.L. Herrera, C.R. del-Bianco, N. García, *Learning 3D structure from 2D images using LBP features*, IEEE International Conference on Image Processing (ICIP), **1**, pp. 2022–2025 (2014).
8. J. Wu, C. Zhang, X. Zhang, Z. Zhang, W.T. Freeman, J.B. Tenenbaum, *Learning shape priors for single-view 3D completion and reconstruction*, CSAIL, Cambridge, MA, USA, pp. 1–10 (2018).
9. J. Konrad, M. Wang, P. Ishwar, C. Wu, D. Mukharjee, *Learning-based, automatic 2D-to-3D image and video conversion*, IEEE Transactions on Image Processing, **22**, *9*, pp. 3485–3496 (2013).
10. R. Parasuraman, R. Varadhan, *Early identification of blood cancer through automated anomaly detection with a convolutional neural network*, Rev. Roum. Sci. Techn. – Électrotechn. et Énerg., **70**, pp. 415–420 (2025).
11. A. Appathurai, A.S.I. Tinu, M. Narayanaperumal, *MEG and PET images-based brain tumor detection using Kapur's Otsu segmentation and sooty optimized Mobilenet classification*, Rev. Roum. Sci. Techn. – Électrotechn. et Énerg., **69**, *3*, pp. 359–364 (2024).
12. National Library of Medicine, *MedlinePlus*, Bethesda, MD, USA, pp. 1–10 (2020).
13. M. Okoli, *Metacarpal bony dimensions related to headless compression screw sizes*, Journal of Hand and Microsurgery, **1**, pp. 39–44 (2020).
14. R. Phan, R. Rzeszutek, D. Androutsos, *Semi-automatic 2D to 3D image conversion using scale-space random walks and a graph cuts based depth prior*, 18th IEEE International Conference on Image Processing, **1**, pp. 865–868 (2011).
15. P. Markelj, D. Tomaževič, B. Likar, F. Pernuš, *A review of 3D/2D registration methods for image-guided interventions*, Medical Image Analysis, **16**, *3*, pp. 642–661 (2012).
16. E.S. Akpan, M. Dauda et al., *Box-Behnken experimental design for the process optimization of catfish bones derived hydroxyapatite: A pedagogical approach*, Materials Chemistry and Physics, **272**, pp. 1–10 (2022).
17. U. Mitrovič, Ž. Špiclin, B. Likar, F. Pernuš, *3D-2D registration of cerebral angiograms, a method and evaluation on clinical images*, IEEE Transactions on Medical Imaging, **32**, pp. 1550–1563 (2013).
18. W. Huang et al., *Toward naturalistic 2D-to-3D conversion*, IEEE Transactions on Image Processing, **24**, pp. 724–733 (2015).
19. A. Ramaiah, P.D. Balasubramanian, A. Appathurai, N.A. Muthukumaran, *Detection of Parkinson's disease via Clifford gradient-based recurrent neural network using multi-dimensional data*, Rev. Roum. Sci. Techn. – Électrotechn. et Énerg., **69**, *1*, pp. 103–108 (2024).
20. E. Menendez-Proupin, S. Cervantes-Rodríguez, R. Osorio-Pulgar, M. Franco-Cisterna, H. Camacho-Montes, M.E. Fuentes, *Computer simulation of elastic constants of hydroxyapatite and fluorapatite*, Journal of the Mechanical Behavior of Biomedical Materials, **4**, *7*, pp. 1011–1020 (2011).
21. D.O. Obada et al., *Fabrication of novel kaolin-reinforced hydroxyapatite scaffolds with robust compressive strengths for bone regeneration*, Applied Clay Science, **1**, pp. 215–224 (2021).
22. E.S. Akpan et al., *A facile synthesis method and fracture toughness evaluation of catfish bones-derived hydroxyapatite*, MRS Advances, **5**, *26*, pp. 1357–1366 (2020).
23. H. Shi, Z. Zhou et al., *Hydroxyapatite-based materials for bone tissue engineering: A brief and comprehensive introduction*, Crystals, **11**, pp. 149–162 (2021).
24. M. Kumar, S. Ramkumar, R. Mageswaran, R. Balakrishnan, *Effective feature extraction method for unconstrained environment: local binary pattern or local ternary pattern*, Rev. Roum. Sci. Techn. – Électrotechn. et Énerg., **69**, *4*, pp. 443–448 (2024).
25. S. Ramkumar, R.K. M. et al., *Programmed for automatic bone disorder clustering based on cumulative calcium prediction for feature extraction*, Clinical Laboratory, **68**, *8*, pp. 1579–1588 (2022).
26. O.A. Osuchukwu, A. Salihi, I. Abdullahi, D.O. Obada et al., *Datasets on the elastic and mechanical properties of hydroxyapatite: A first principle investigation, experiments, and pedagogical perspective*, Data in Brief, **48**, pp. 1–11 (2023).
27. R.I. Martin, P.W. Brown, *Mechanical properties of hydroxyapatite formed at physiological temperature*, Journal of Materials Science: Materials in Medicine, **6**, pp. 138–143 (1995).
28. E. Menendez-Proupin, S. Cervantes-Rodríguez, R. Osorio-Pulgar, M. Franco-Cisterna, H. Camacho-Montes, M.E. Fuentes, *Computer simulation of elastic constants of hydroxyapatite and fluorapatite*, Journal of the Mechanical Behavior of Biomedical Materials, **4**, *7*, pp. 1011–1020 (2011).
29. I. Ielo, G. Calabrese, G. De Luca, S. Conoci, *Recent advances in hydroxyapatite-based biocomposites for bone tissue regeneration in orthopedics*, International Journal of Molecular Sciences, **23**, *17*, pp. 9721–9733 (2022).
30. Z. Li, Q. Wang, G. Liu, *A review of 3D printed bone implants*, Micromachines, **13**, pp. 1–25 (2022).